Materials Chemistry and Physics 192 (2017) 260–267

Contents lists available at ScienceDirect

Materials Chemistry and Physics

journal homepage: www.elsevier.com/locate/matchemphys

Electronic structure and optical properties of β-RbSm$(MoO_4)_2$ from spin polarization calculations: DFT+U

A.H. Reshak [a, b, *]

[a] New Technologies - Research Centre, University of West Bohemia, Univerzitni 8, 306 14 Pilsen, Czech Republic
[b] School of Material Engineering, University Malaysia Perlis, 01007 Kangar, Perlis, Malaysia

HIGHLIGHTS

- Influence of inclusion the spin polarization on the gap of β-RbSm$(MoO_4)_2$.
- Sm-4f in spin-up CBM causes a significant influence on properties of β-RbSm$(MoO_4)_2$.
- β-RbSm$(MoO_4)_2$ exhibits positive and negative uniaxial anisotropy.

ARTICLE INFO

Article history:
Received 30 December 2015
Received in revised form
29 July 2016
Accepted 1 February 2017
Available online 2 February 2017

Keywords:
Electronic materials
Inorganic compounds
Optical materials
Ab initio calculations
Band-structure
Crystal structure

ABSTRACT

We explored the influence of the inclusion of spin polarization on the energy band gap of β-RbSm$(MoO_4)_2$. Calculations explored that the appearance of Sm-4f states at the conduction band minimum (CBM) of the spin-up case causes a significant influence on ground state properties of β-RbSm$(MoO_4)_2$. The total and partial densities of states confirm the existence of Sm-4f states in the CBM of the spin-up case. The partial densities of states exhibit a strong hybridization between some states which may lead to the formation of covalent bonds. The valence band maximum (VBM) and the CBM are located at the center of first Brillouin zone (Γ), resulting in a direct band gap for both of majority spin (↑) and minority spin (↓). The values of the band gap are 3.01 eV (↑) and 3.78 eV (↓). The all-electron full potential linear augmented plane wave (FPLAPW+lo) method within the generalized gradient approximation plus the Hubbard Hamiltonian (GGA+U) were used. We have applied U on 4*f* orbital of Sm atoms and 4*d* orbital of Mo atoms. We have taken a careful look at the electronic charge density distribution to visualize the charge transfer and the chemical bonding characters. The calculated bond lengths show very good agreements with the measured ones. The optical properties were calculated to seek a deep insight into the electronic structure. It has been found that below λ = 450 nm β-RbSm$(MoO_4)_2$ exhibits a positive uniaxial anisotropy, while at λ = 450 nm and above, the crystal exhibits a negative uniaxial anisotropy.

1. Introduction

The magnetic semiconductors are very promising materials for optoelectronic and spintronics applications [1–5]. Different magnetic semiconductors compounds have been intensively studied theoretically as well as experimentally to design efficient devices like super smart diodes, super smart memory chips, spin valves and spin field effect transistors [6–14]. It is essential to explain the known properties of a given material designed for the fabrication of highly efficient electronic and spintronics devices and even to predict different properties of hypothetical materials.

Due to their interesting structural, physical, chemical, luminescent and spectroscopic properties, the molybdate crystals have become potential candidates for enormous application in photochemistry, optical technologies [15–22], laser applications and electronics [23–28]. Among them the rare-earth containing crystals particularly β-RbSm$(MoO_4)_2$. Recently, Atuchin et al. [29,30] have synthesized β-RbSm$(MoO_4)_2$ and investigated the chemical bonding, structural and vibrational properties. They found that the crystal structure of rubidium samarium dimolybdate consists of layers of MoO_4 tetrahedrons corner-sharing with SmO_8 square

* New Technologies - Research Centre, University of West Bohemia, Univerzitni 8, 306 14 Pilsen, Czech Republic.
E-mail address: maalidph@yahoo.co.uk.

http://dx.doi.org/10.1016/j.matchemphys.2017.02.011
0254-0584/

antiprisms. The rubidium samarium dimolybdate was found in quasi-binary system $Rb_2MoO_4Sm_2(MoO_4)_3$ with Rb:Sm of 1:1 below the temperature 890-910° C [30]. The earlier reported β ↔ α phase transition at T ~ 860–910 °C was not verified [30]. It has been reported that the electronic structure properties of β-$RbSm(MoO_4)_2$ remains unknown [30]. This motivated us to perform a first principle calculation for β-$RbSm(MoO_4)_2$ based on density functional theory (DFT) to investigate the electronic band structure. In our previous work [31] we have performed calculation on β-$RbNd(MoO_4)_2$ which show that the band gap differences between spin-up/down cases is about 0.067 eV; therefore, the system show no favorable spin channel. It is interested to highlight that in β-$RbNd(MoO_4)_2$ the conduction band minimum (CBM) for spin-up/down is formed by Mo-d states. In the current work we are interested in replacing Nd by Sm to investigate the influence of this replacement on the band structure. Since Sm possesses higher electronegativity than Nd, we expected that replacing Nd by Sm will lead to a shift of Sm-4f band of the spin-up case towards lower energies [32]. Such a shift will cause significant influence on the electronic band structure and hence the optical properties.

To the best of our knowledge there is lack of information about the electronic structure, optical properties and the electron charge density distribution of the β-$RbSm(MoO_4)_2$. Also, there is no spin polarization calculation for β-$RbSm(MoO_4)_2$ in the literature. Therefore, as a natural extension to existence information, a detailed depiction of the structural, electronic, and optical properties using full potential method is timely and would bring us important insights in understanding the band structure and optical properties. Hence it is very important to use the all-electron full-potential linear augmented plane wave (FPLAPW+lo) method plus Hubbard Hamiltonian to investigate the spin polarized electronic band structure, density of states, the electron charge density distribution and the optical properties. In the recent years, due to the improvement of the computational technologies, it has been proven that the first-principles calculation is a strong and useful tool to predict the crystal structure and its properties related to the electron configuration of a material before its synthesis [33–36].

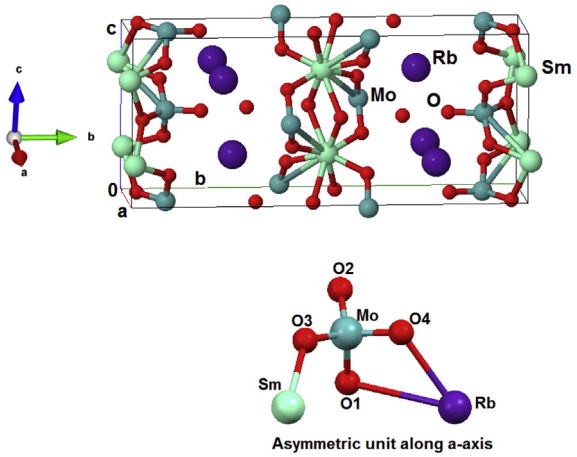

Fig. 1. The crystal structure of β-$RbSm(MoO_4)_2$.

2. Details of calculation

It has been reported that β-$RbSm(MoO_4)_2$ crystallized in orthorhombic symmetry of *Pbcn* space group. β-$RbSm(MoO_4)_2$ consists of eight formula per unit cell [29]. The reported lattice parameters are a = 5.1431(2) Å, b = 18.8195(7) Å and c = 8.1641(3) Å [29]. The crystal structure of the orthorhombic β-$RbSm(MoO_4)_2$ consists of complex layers. These layers are formed by MoO_4 tetrahedrons shared by corners with Sm_8 square antiprisms as shown in Fig. 1. The following states are considered as valence electrons, ($4s^2\ 4p^6\ 5s^1$), ($5s^2\ 5p^6\ 4f^6\ 6s^2$), ($4d^5\ 5s^1$) and ($2s^2\ 2p^4$) for Rb, Sm, Mo and O, respectively. We have used the experimental crystallographic data reported by Atuchin et al. [29] as starting point of these calculations. Using the full potential linear augmented plane wave (FPLAPW+lo) method as implemented in WIEN2k package [37] within the generalized gradient approximation (PBE+GGA) [38], the experimental structural geometry was optimized. The

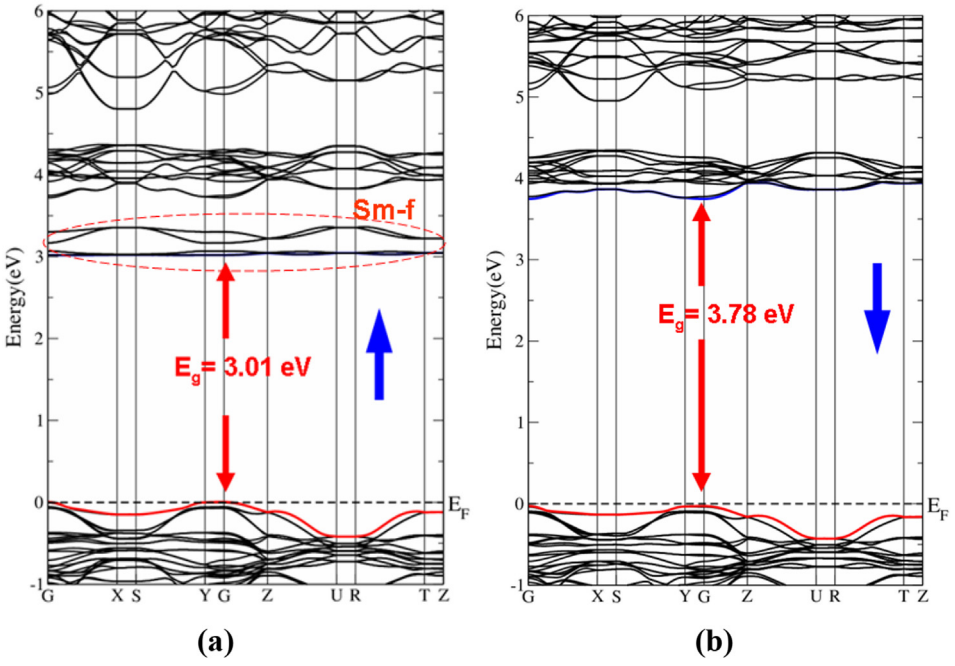

Fig. 2. Calculated electronic band structure of β-$RbSm(MoO_4)_2$; (a) spin-up case; (b) spin-down case.

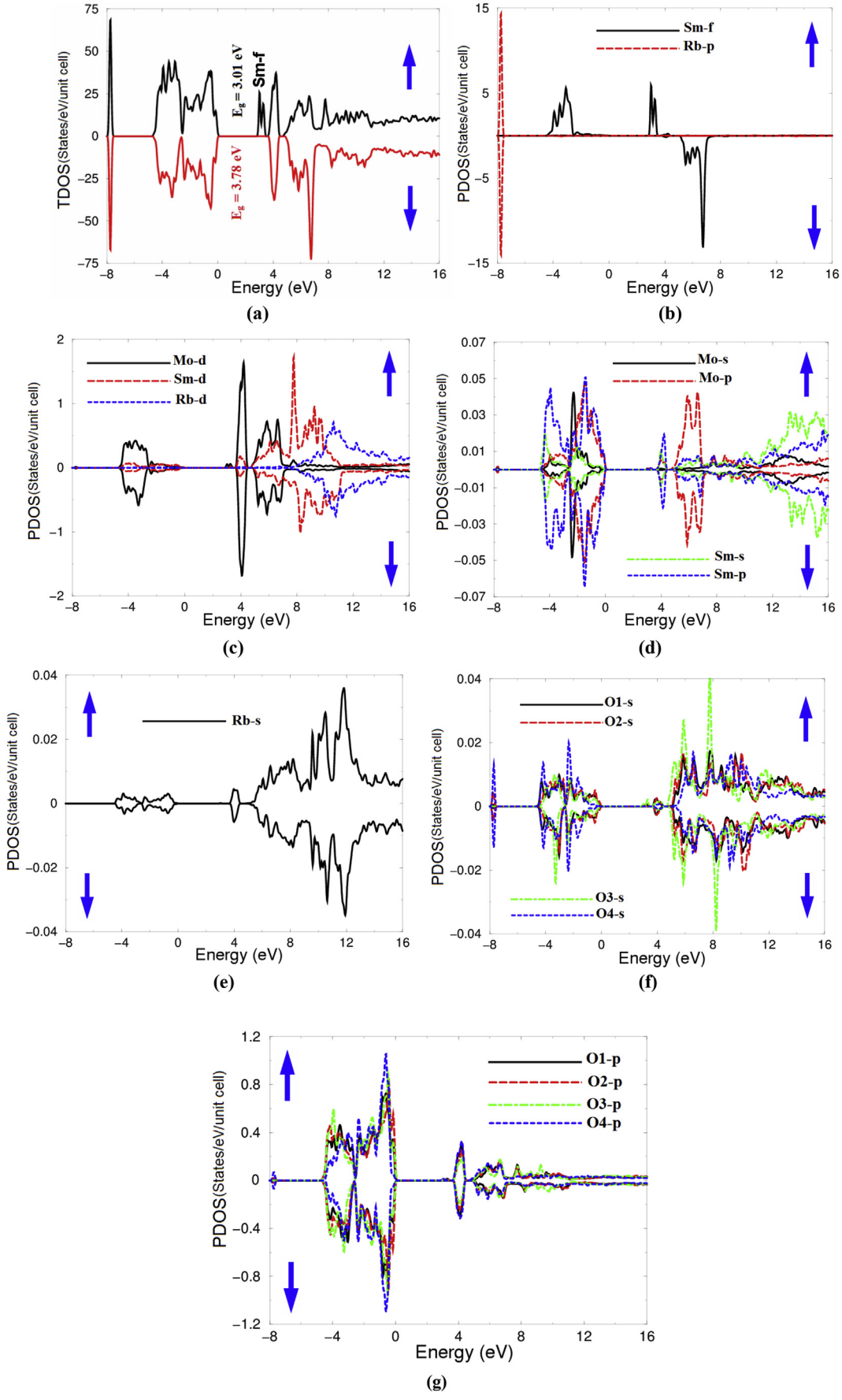

Fig. 3. Calculated total and partial densities of states for spin-up/down.

Table 1
Calculated atom-resolved spin magnetic moments (in μB).

Mo (μB)	Sm (μB)	Rb (μB)	O1 (μB)	O2 (μB)	O3 (μB)	O4 (μB)	Interst. (μB)
0.00068	4.96346	−0.00005	−0.00714	−0.00489	−0.00782	−0.00084	0.30672

atomic positions were relaxed by minimizing the forces acting on each atom; we assume that the structure is totally relaxed when the forces on each atom reach values less than 1 mRy/a.u. From the obtained, relaxed geometry the electronic structure, the chemical bonding, electronic charge density and the optical properties have been determined using FPLAPW+lo [39–41] within GGA+U, where U is the Hubbard Hamiltonian. We have applied U on 4*f* orbital of Sm atoms and 4*d* orbital of Mo atoms, the U values are 6.0 eV and 3.0 eV respectively [30]. As there are no experimental measurements of U for this compound, we have decided to perform calculations for various values of U and keeping the J parameter fixed at 0.05 Ry because U increases with increasing nuclear charge and valence state, whereas J is almost independent of the number of n*d* (n*f*) electrons. The main motivation for taking different U values is to find which U value gives the best fit to the measured energy gap. We take the full relativistic effects for core states and use the scalar relativistic approximation for the valence states. More details regarding the use of different values of U are found elsewhere [42]. The details of the spin polarized FPLAPW+lo method are presented elsewhere [43]. The potential for the construction of basis functions inside the sphere of the muffin tin was spherically symmetric, whereas outside the sphere it was constant [43]. The total and partial density of states (DOS) were calculated by means of the modified tetrahedron method [44]. The input data required for calculating the DOS are the energy eigenvalues and eigenfunctions which are the natural outputs of a band structure calculation. The total DOS and partial DOS are calculated for a large energy range (−8.0 eV up to 16.0 eV). The states below the Fermi energy (E_F) are the valence states and states above E_F are the conduction states. Hence, we obtain DOS for both valence and conduction band states. Self-consistency is obtained using 300 $\vec{k}$ points in the irreducible Brillouin zone (IBZ). The self-consistent calculations are converged since the total energy of the system is stable within 0.00001 Ry. The electronic band structure and the related properties were performed within 600 $\vec{k}$ points in the IBZ.

3. Results and discussion

3.1. Spin polarized electronic band structure and density of states

The calculated spin-polarized electronic band structure of β-$RbSm(MoO_4)_2$ for majority spin (↑) and minority spin (↓) are illustrated in Fig. 2(a) and (b). For both cases the zero of the energy scale is taken at the top of the valence band. The valence band maximum (VBM) and the CBM are located at the center of the first BZ, resulting in a direct band gap for both of majority spin (↑) and minority spin (↓). The values of the band gap are 3.01 eV (↑) and 3.78 eV (↓). It is clear that in the majority spin, the bands around 3.0 eV belong to Sm-4f orbital which govern the CBM. These bands vanish in minority spin case (↓) to lead to an increase of the band gap and the CBM is formed by Mo-4d orbitals. It is clear that the majority spin (↑) state contains more electrons than the minority spin (↓) state.

In order to have better insight into the electronic structure, we have presented and explained the necessary ingredients of the calculated total and atom-resolved density of states as shown in Fig. 3(a)–(g). Fig. 3(a) presents the total density of states (TDOS) for the majority and minority spin which explored the differences between the two cases, as it is clear both structures are similar expect that the majority spin exhibit extra structure which belongs to Sm-4f orbital. This orbital form the CBM for (↑) while Mo-4d orbital forms the CBM of (↓) in agreement with the previous observation from the electronic band structure (Fig. 2). This finding confirms our expectation that replacing Nd by Sm leads to a shift of Sm-4f bands of spin-up case towards lower energies, resulting in a reduction of the spin-up band gap and shows that the spin-up case of β-$RbSm(MoO_4)_2$ is a favorable spin channel.

From the angular momentum projected density of states (PDOS) we are able to identify the angular momentum character of the various structures. The structure around −8.0 eV belongs to Rb-4p state for (↑) and (↓). The structure extend from −3.0 eV up to Fermi level (E_F) is mainly originated from Sm-4f, Mo-4d states, with small contributions from Mo-5s/4p, Sm-6s/5p/4d, Rb-5s/3d and O-2s/2p states for (↑) case. Whereas for (↓) case, the same states contribute except the Sm-4f state that exhibits zero contribution. The energy region above E_F is very broad. For the (↑) case, this region extend between 3.01 eV and above whereas for (↓) case, it is between 3.78 eV and above. In both cases (majority and minority spin) the energy region above E_F is formed by Mo-5s/4p/4d, Sm-6s/5p/4d, Rb-5s/3d and O-2s/2p states. The spin magnetic moments are calculated for the atom resolved within the muffin-tin spheres as well as in the interstitial sites as shown in Table 1. The calculated spin magnetic moments are in accordance with Slater-Pauling rule. Calculations show that the magnetic moment of 4f electrons within Sm sphere is about 4.963 μB. Fig. 3(f) show that the 2s-state of the four O atoms hybridized strongly among each other along the whole energy range for spin up/down; they also hybridized with Rb-5s state (Fig. 3e) in the energy region form 4.5 eV and above. The hybridization may lead to the formation of partial covalent bonds between O and Rb atoms depending on the degree of the hybridization. The 2p-states of the four O atoms hybridize strongly among each other along the whole energy range for spin up/down as shown in Fig. 3(g). The PDOS helps to identify the bonds characters between the atoms. To support this observation, we have taken a careful look at the valence band's electronic charge density distribution to visualize the charge transfer and the chemical bonding characters. Fig. 4(a–d) illustrated the calculated total valence charge density distribution in (1 0 0) and (1 0 1) crystallographic planes for spin-up and spin-down cases. According to Pauling scale, the electro-negativity of Rb, Sm, Mo and O atoms are 0.82, 1.17, 2.16 and 3.44, respectively. Therefore, due to the electro-negativity differences between the atoms, some valence electrons are transferred towards O atoms as it is clear that the O atoms are surrounded by uniform blue spheres (indicate the maximum charge accumulation). For both cases (spin up/down), Rb, Mo and Sm atoms form partial covalent bonds with O atoms. It is clear from (1 0 0) and (1 0 1) crystallographic planes that all atoms are surrounding by a uniform spherical charge and Rb, Sm and Mo atoms share their outer shells with O atoms to form partially covalent and mostly ionic bonds. The calculated bond lengths are listed in Table 2 and compared to the measured bonds distance at room temperature [29]; good agreement was found. It is clear that Mo atom form the shortest bonds with O atoms. The bond lengths and the two crystallographic planes explore the anisotropy of β-$RbSm(MoO_4)_2$ for the majority spin (↑) and minority spin (↓).

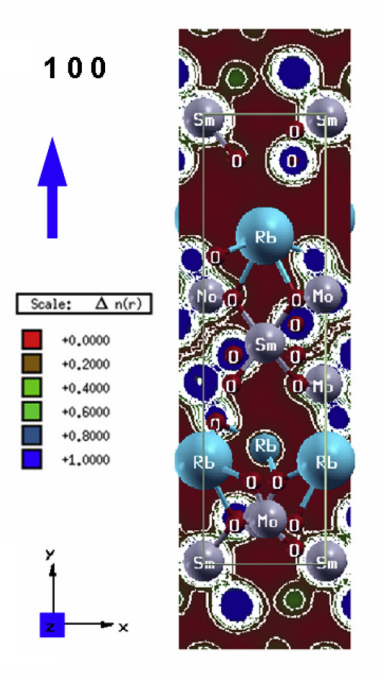

(a) Crystallographic plane (1 0 0) for spin-up

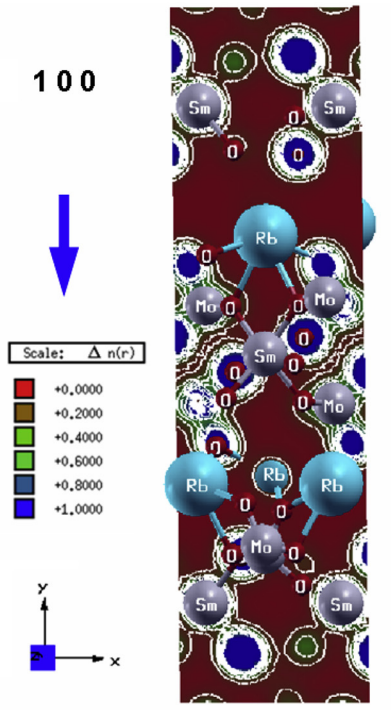

(b) Crystallographic plane (1 0 0) for spin-down

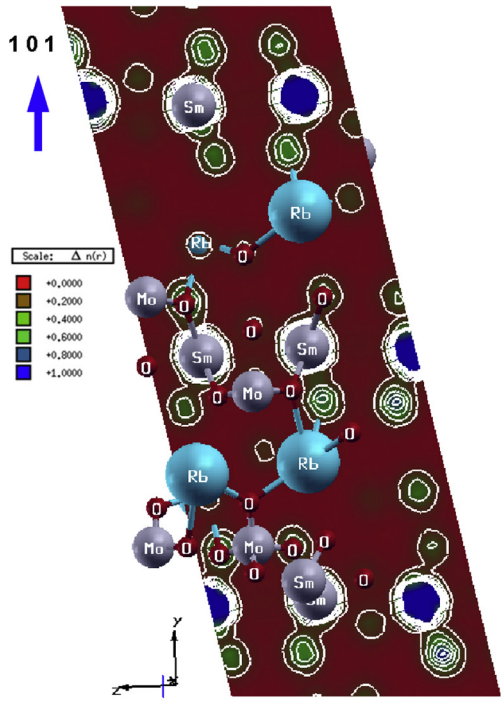

(c) Crystallographic plane (1 0 1) for spin-up

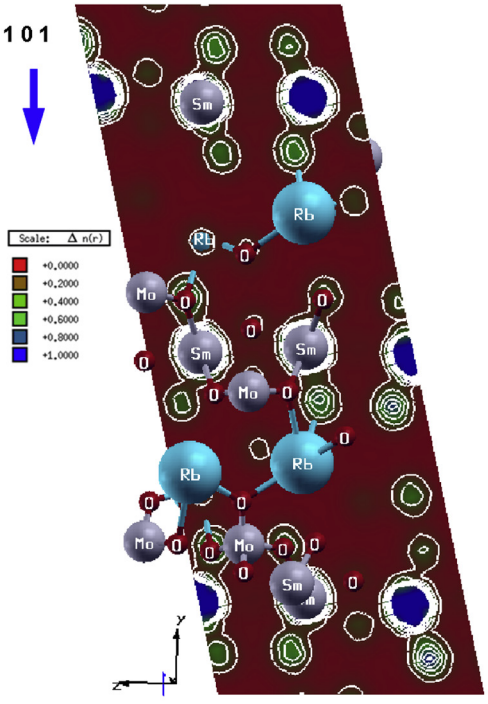

(d) Crystallographic plane (1 0 1) for spin-down

Fig. 4. Calculated electronic charge density distribution**; (a)** crystallographic plan (1 0 0) for spin-up case; **(d)** crystallographic plan (1 0 0) for spin-down case; **(c)** crystallographic plan (1 0 1) for spin-up case; **(d)** crystallographic plan (1 0 1) for spin-down case.

3.2. Linear optical properties

Deep insight into the electronic structure can be obtained from calculating and analyzing the optical properties. The dispersion of the imaginary part of the optical dielectric function were calculated for spin-up and spin-down to ascertain the influence of the spin polarization on the optical properties as shown in Fig. 5(a). It has been noted that the first critical points (the absorption edges) for the

Table 2
The calculated inter-atomic distances in comparison with the measured ones at room temperature [29].

Bond	Bond Lengths (Å)	
	Exp.	Calc.
Rb–O1	2.75(2)	2.74
Rb–O2	3.03(4)	3.04
Rb–O3	2.98(2)	2.99
Rb–O4	2.75(2)	2.74
Sm–O1	2.35(4)	3.34
Sm–O2	2.31(3)	2.32
Sm–O3	2.61(4)	2.60
Sm–O4	2.44(4)	2.45
Mo–O1	1.82(3)	1.83
Mo–O2	1.74(2)	1.75
Mo–O3	1.83(2)	1.82
Mo–O4	1.70(2)	1.71

three compounds $\varepsilon_2^{xx}(\omega)$, $\varepsilon_2^{yy}(\omega)$ and $\varepsilon_2^{zz}(\omega)$ of the imaginary part of the optical dielectric function along the polarizations directions [1 0 0], [0 1 0] and [0 0 1] are located at 3.01 eV (3.78 eV) for the spin-up (spin-down). Overall the optical spectral structures of spin-up/down are similar except for minor differences in spin-up case that are attributed to the difference in energy gap values and the existence of Sm-4f extra structure around −4.0 eV below E_F and the position of Sm-4f around +3.01 eV above E_F. This causes significant influence on the optical properties. The first spectral structure occurs due to the transitions between the states just below and above E_F. Therefore, Sm-4f state (around 3.01 eV) cause significant influence on the optical properties for the spin-up case in comparison to the spin-down case. The spectral structure confined between 6.0 and 9.0 eV is due to the optical transitions from Sm-6s/5p/4f, Mo-5s/4p/4d and O-2s/2p states to Sm-5p/4d, Mo-4p/4d, Rb-5s and O-2s/2p states. This spectral structure clearly illustrates the influence of the existence of Sm-4f extra structure in spin-up case only. The three optical tensor components exhibit a considerable anisotropy. The last structure (9.0 up to 13.5 eV) exhibits the lossless regions. We have used the Kramers-Kronig transformation [45] to obtain the real parts of the optical dielectric functions. The calculated real parts along the polarizations directions [1 0 0], [0 1 0] and [0 0 1] are presented in Fig. 5(b). We can see that the structure confined between 6.0 and 9.0 eV exhibit minor differences in spin-up case than that of spin-down case in concordance with our observation from the imaginary part (Fig. 5(a)). The values of $\varepsilon_1^{xx}(0)$, $\varepsilon_1^{yy}(0)$ and$\varepsilon_1^{zz}(0)$ are calculated for the spin-up and spin-down cases. Also, we have calculated the values of $\varepsilon_1^{xx}(\omega)$, $\varepsilon_1^{yy}(\omega)$ and$\varepsilon_1^{zz}(\omega)$ at λ = 400, 450 and 800 nm. These values are presented in Table 3. We note that a smaller energy gap yields a larger $\varepsilon_1(0)$ value. This could be explained on the basis of the Penn model [46]. Penn proposed a relation between $\varepsilon(0)$ and E_g, $\varepsilon(0) \approx 1 + (\hbar\omega_P/E_g)^2$. E_g is some kind of averaged energy gap which could be related to the real energy gap. It is clear that $\varepsilon(0)$ depends on $1/E_g^2$. Hence, a larger E_g yields a smaller $\varepsilon(0)$. Therefore, the values of $\varepsilon_1^{xx}(\omega)$, $\varepsilon_1^{yy}(\omega)$ and$\varepsilon_1^{zz}(\omega)$ for the spin-down case are smaller than those for of spin-up case. In addition, We have calculated the uniaxial anisotropy$\delta\varepsilon = [(\varepsilon_0^{II} - \varepsilon_0^{\perp})/\varepsilon_0^{tot}]$ [47,48] for spin-up and spin-down cases at the static limit, λ = 400, 450, and 800 nm. These values are listed in Table 3, indicating the existence of a considerable anisotropy. It is clear that below λ = 450 nm, β-RbSm$(MoO_4)_2$ exhibits positive uniaxial anisotropy while at λ = 450 nm and above, the crystal exhibits negative uniaxial anisotropy, in good agreement

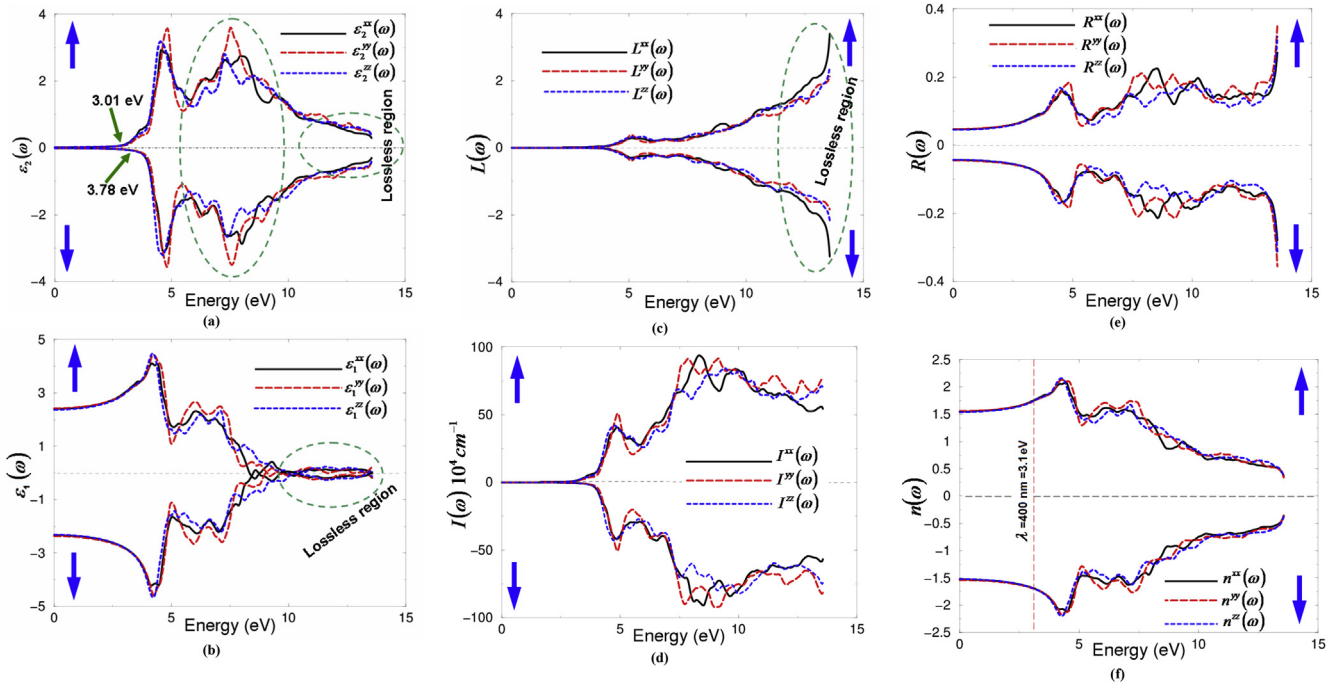

Fig. 5. (a). Calculated $\varepsilon_2^{xx}(\omega)$ (**dark solid curve-black color online**),$\varepsilon_2^{yy}(\omega)$ (light dashed curve-red color online) and $\varepsilon_2^{zz}(\omega)$ (light solid curve-blue color online) spectra for spin-up/down (b). Calculated $\varepsilon_1^{xx}(\omega)$ (**dark solid curve-black color online**), $\varepsilon_1^{yy}(\omega)$ (light dashed curve-red color online) and $\varepsilon_1^{zz}(\omega)$ (light solid curve-blue color online) spectra for spin-up/down; (c). Calculated $L^{xx}(\omega)$ (**dark solid curve-black color online**), $L^{yy}(\omega)$ (light dashed curve-red color online) and $L^{zz}(\omega)$ (light solid curve-blue color online) spectra for spin-up/down; (d) Calculated absorption coefficient $I^{xx}(\omega)$ (**dark solid curve-black color online**), $I^{yy}(\omega)$ (light dashed curve-red color online) and $I^{zz}(\omega)$ (light solid curve-blue color online) spectrum. The absorption coefficient in 10^4 sec^{-1}; (e). Calculated $R^{xx}(\omega)$ (**dark solid curve-black color online**), $R^{yy}(\omega)$ (light dashed curve-red color online) and $R^{zz}(\omega)$ (light solid curve-blue color online) spectra for spin-up/down; (f). Calculated $n^{xx}(\omega)$ (**dark solid curve-black color online**), $n^{yy}(\omega)$ (light dashed curve-red color online) and $n^{zz}(\omega)$ (light solid curve-blue color online) spectra for spin-up/down. (For interpretation of the references to colour in this figure legend, the reader is referred to the web version of this article.)

Table 3
Calculated $\varepsilon_1^{xx}(\omega)$, $\varepsilon_1^{yy}(\omega)$, $\varepsilon_1^{zz}(\omega)$, $\varepsilon_1^{tot}(\omega)$, $\delta\varepsilon$, $n^{xx}(\omega)$, $n^{yy}(\omega)$, $n^{zz}(\omega)$, $\hbar\omega_p^{xx}$, $\hbar\omega_p^{yy}$, and $\hbar\omega_p^{zz}$ at static limit, λ = 400, 450, and 800 nm. $\hbar\omega_p^{xx}$, $\hbar\omega_p^{yy}$, and $\hbar\omega_p^{zz}$ are calculated in eV.

Components	At static limit		At λ = 400 nm		At λ = 450 nm		At λ = 800 nm	
	Spin-up	Spin- down	Spin-up	Spin- down	Spin- up	Spin- down	Spin-up	Spin- down
$\varepsilon_1^{xx}(\omega)$	2.403	2.327	3.081	2.846	2.850	2.689	2.512	2.421
$\varepsilon_1^{yy}(\omega)$	2.425	2.361	3.045	2.868	2.832	2.716	2.528	2.454
$\varepsilon_1^{zz}(\omega)$	2.374	2.312	3.060	2.853	2.815	2.687	2.482	2.408
$\varepsilon_1^{tot}(\omega)$	2.40	2.333	3.062	2.855	2.832	2.697	2.507	2.427
$\delta\varepsilon$	0.0166	0.0137	0.0083	0.0050	−0.0093	−0.0085	−0.0027	−0.0162
$n^{xx}(\omega)$	1.549	1.526	1.754	1.891	1.688	1.639	1.584	1.556
$n^{yy}(\omega)$	1.557	1.536	1.746	1.883	1.682	1.648	1.589	1.568
$n^{zz}(\omega)$	1.540	1.520	1.745	1.882	1.677	1.639	1.573	1.550
$\hbar\omega_p^{xx}$	8.340	8.503	8.340	8.503	8.340	8.503	8.340	8.503
$\hbar\omega_p^{yy}$	9.102	9.047	9.102	9.047	9.102	9.047	9.102	9.047
$\hbar\omega_p^{zz}$	10.027	13.401	10.027	13.401	10.027	13.401	10.027	13.401

with the previous work [30]. There are other features in the optical spectrum, such as plasmon oscillations, which are associated with inter-band transitions. The plasmon maximum is usually the most intense feature in the spectrum and this is at energy where $\varepsilon_1^{xx}(\omega)$, $\varepsilon_1^{yy}(\omega)$ and$\varepsilon_1^{zz}(\omega)$ crosses zero which is associated with the existence of plasma oscillations. The plasma frequency (energy) is calculated and presented in Table 3.

The loss function of β-RbSm$(MoO_4)_2$ as function of photon energy is illustrated in Fig. 5(c). We can see that the spectral structure of $L^{xx}(\omega)$, $L^{yy}(\omega)$ and$L^{zz}(\omega)$ is almost zero along the energy range up to 9.0 eV. Then a rapid increase occurs at higher energies which represent the plasma frequencies (ω_p) and confirm the existence of the lossless regions in concordance with our observation in Fig. 5(a) and (b).

The absorption coefficients as shown in Fig. 5(d) exhibit that the absorption edge of spin-up case is lower than that of spin-down case, confirming that the spin-up case possess a smaller energy gap as compared to the spin-down case. The absorption spectral structure shows three absorption regions; the low absorption region extends from the fundamental energy band gap up to 6.0 eV; the high absorption region (6.0 up to 11.0 eV); and another low absorption region from 11.0 eV and above. β-RbSm$(MoO_4)_2$ exhibits low reflectivity almost 20% along the whole energy range as illustrated in Fig. 5(e). The reflectivity minima occur around 12.0 eV confirming the occurrence of collective plasmon resonance which represents the lossless regions.

In addition, we have calculated the refractive indices $n^{xx}(\omega)$, $n^{yy}(\omega)$ and $n^{zz}(\omega)$ for spin-up and spin-down as shown in Fig. 5(f). The values of the refractive indices at the static limit, λ = 400 nm, λ = 450 nm and λ = 850 nm, are listed in Table 3. The calculated values of $n^{xx}(\omega)$, $n^{yy}(\omega)$ and $n^{zz}(\omega)$ at λ = 400 nm show reasonable agreement with the previous work [30] obtained by using LDA+U. The refractive indices have direct relation with the energy band gap $(n = \sqrt{\varepsilon})$ therefore, we can estimated the value of the energy band gap from calculated values of the refractive indices.

4. Conclusions

The all-electron full potential linear augmented plane wave (FPLAPW+lo) method and the generalized gradient approximation plus the Hubbard Hamiltonian (GGA+U) were used to calculated the spin polarized electronic band structure, density of states, the chemical bonding and the optical properties of β-RbSm$(MoO_4)_2$. We have applied *U* on 4*f* orbital of Sm atoms and 4*d* orbital of Mo atoms. Calculations show that β-RbSm$(MoO_4)_2$ is a direct band gap semiconductor for spin-up and spin-down cases. The spin-up case exhibits a smaller band gap than that obtained from the spin-down case; that is attributed to the appearance of Sm-4f states on the conduction band minimum of the spin-up case. We have calculated total valence charge density distribution in (1 0 0) and (1 0 1) crystallographic planes for spin-up and spin-down cases. The calculated bond lengths show very good agreements with the measured one. The optical properties show there exists a lossless region and considerable anisotropy. It has been found that the β-RbSm$(MoO_4)_2$ crystal exhibits positive uniaxial anisotropy below λ = 450 nm and negative uniaxial anisotropy above λ = 450 nm, in agreement with previous work of Atuchin et al. The good agreement with experimental data indicates the accuracy of the method used here.

Acknowledgments

The result was developed within the CENTEM project, reg. no. CZ.1.05/2.1.00/03.0088, cofunded by the ERDF, as part of the Ministry of Education, Youth and Sports OP RDI programme and the follow-up sustainability stage, supported through CENTEM PLUS (LO1402) by the Ministry of Education, Youth and Sports, under the "National Sustainability Programme I. Computational resources were provided by MetaCentrum (LM2010005) and CERIT-SC (CZ.1.05/3.2.00/08.0144) infrastructures.

References

[1] S. Koshihara, A. Oiwa, M. Hirasawa, S. Katsumoto, Y. Iye, C. Urano, H. Takagi, H. Munekata, Phys. Rev. Lett. 78 (1997) 4617.
[2] H. Ohno, D. Chiba, F. Matsukura, T. Omiya, E. Abe, T. Dietl, Y. Ohno, K. Ohtani, Nat. Lond. 408 (2000) 944.
[3] M. Idrish Miah, I.V. Kityk, E. Mac, A. Gray, Acta Mater. 55 (2007) 6392.
[4] Q.J. Feng, D.Z. Shen, J.Y. Zhang, B.H. Li, Z.Z. Zhang, Y.M. Lu, X.W. Fan, Mater. Chem. Phys. 112 (2006) 1106.
[5] J. Luengo, N.V. Joshi, Mater. Lett. 25 (1995) 65.
[6] B. Amin, Iftikhar Ahmad, M. Maqbool, S. Goumri-Said, R. Ahmad, J. Appl. Phys. 109 (2011) 023109.
[7] B. Amin, I. Ahmad, M. Maqbool, J. Light Wave Technol. 28 (2010) 223.
[8] S. Drablia, H. Meradji, S. Ghemid, S. Labidi, B. Bouhafs, Phys. Scr. 79 (2009) 045002.
[9] Y.K. Kuo, B.T. Liou, S.H. Yen, H.Y. Chu, Opt. Commun. 237 (2004) 363–369.
[10] R. de Paiva, J.L.A. Alves, R.A. Nogueira, C. de Oliveira, H.W.L. Alves, L.M.R. Scolfaro, J.R. Leite, Mater. Sci. Eng. B 93 (1–3) (2002) 25–30.
[11] Y.A. Pusep, M.T.O. Silva, J.R.L. Fernandez, V.A. Chitta, J.R. Leite, T. Frey, D.J. As, D. Schikora, K. Lischka, J. Appl. Phys. 91 (2002) 6197–6199.
[12] E. Martinez-Guerrero, E.B. Amalric, L. Martinet, G. Feuillet, B. Daudin, H. Mariette, P. Holliger, C. Dubois, C. Bru-Chevallier, P. Nze, T. AbougheChassagne, G. Ferro, Y. Monteil, J. Appl. Phys. 91 (2002) 4983–4987.
[13] E. Martinez-Guerrero, C. Adelmann, F. Chabuel, J. Simon, N.T. Pelekanos, G. Mula, B. Daudin, G. Feuillet, H. Mariette, Appl. Phys. Lett. 77 (2000) 809.
[14] H. Okumura, H. Hamaguchi, T. Koizumi, K. Balakrishnan, Y. Ishida, M. Arita, S. Chichibu, H. Nakanishi, T. Nagatomo, S. Yoshida, J. Cryst. Growth 390 (1998) 189–190.
[15] T.T. Basiev, A.A. Sobol, Yu.K. Voronko, P.G. Zverev, Opt. Mater. 15 (2000) 205–216.

[16] Z.L. Gao, X.T. Tao, X. Yin, W.G. Zhang, M.H. Jiang, Appl. Phys. Lett. 93 (2008) 252906.
[17] G.P. Cai, J.Y. Wang, H.J. Zhang, Cryst. Res. Technol. 44 (2009) 1001–1004.
[18] M. Mączka, A. Pietraszko, W. Paraguassu, A.G. Souza Filho, P.T.C. Freire, J. Mendes Filho, P.T.C. Freire, J. Mendes Filho, J. Hanuza, J. Phys. Condens Matter 21 (2009) 095402.
[19] T. Namsaraeva, B. Bazarov, D. Mikhailova, N. Kuratieva, A. Sarapulova, A. Senyshyn, et al., Eur. J. Inorg. Chem. (2011) 2832–2841.
[20] J.J. Zhang, Z.L. Gao, X. Yin, Z.H. Zhang, Y.X. Sun, X.T. Tao, Appl. Phys. Lett. 101 (2012) 062901.
[21] V.V. Atuchin, V.G. Grossman, S.V. Adichtchev, N.V. Surovtsev, T.A. Gavrilova, B.G. Bazarov, Opt. Mater. 34 (2012) 812–816.
[22] C.S. Lim, Mater Res. Bull. 47 (2012) 4220–4225.
[23] P.V. Klevtsov, R.F. Klevtsova, J. Struct. Chem. 18 (3) (1977) 419.
[24] T.T. Basiev, A.A. Sobol, Yu. K. Voronko, P.G. Zverev, Opt. Mater. 15 (2000) 205.
[25] F.E. Osterloh, Chem. Mater. 20 (2008) 35.
[26] A. Kudo, Y. Miseki, Chem. Soc. Rev. 38 (2009) 253.
[27] M. Maczka, A.G. Souza Filho, W. Paraguassu, P.T.C. Freire, J. Mendes Filho, J. Hanuza, Prog. Mater. Sci. 57 (2012) 1335.
[28] O.D. Chimitova, V.V. Atuchin, B.G. Bazarov, M.S. Molokeev, Z.G. Bazarova, Proc. SPIE 8771 (2013) 87711A.
[29] V.V. Atuchin, O.D. Chimitova, S.V. Adichtchev, J.G. Bazarov, T.A. Gavrilova, M.S. Molokeev, N.V. Surovtsev, Zh.G. Bazarova, Mater. Lett. 106 (2013) 26–29.
[30] V.V. Atuchin, A.S. Aleksandrovsky, O.D. Chimitova, Cheng-Peng Diao, T.A. Gavrilova, V.G. Kesler, M.S. Molokeev, A.S. Krylov, B.G. Bazarov, J.G. Bazarova, Zheshuai Lin, Dalton Trans. 44 (2015) 1805.
[31] A.H. Reshak, RSC Adv. 5 (2015) 44960.
[32] Joo-Hyoung Lee, J. Wu, J.C. Drossman, Phys. Rev. Lett. 104 (2010) 016602.
[33] K.J. Plucinski, I.V. Kityk, J. Kasperczyk, B. Sahraoui, Semicond. Sci. Technol. 16 (2001) 467–470.
[34] M. Malachowski, I.R. Kityk, B. Sahraoui, Phys. Lett. A 242 (1998) 337–342.
[35] A.H. Reshak, A. Majchrowski, M. Swirkowicz, A. Kłos, T. Łukasiewicz, I.V. Kityk, K. Iliopoulos, S. Couris, M.G. Brik, J. Alloys Compd. 481 (2009) 14–16.
[36] A.H. Reshak, S. Auluck, I.V. Kityk, J. Alloys Compd. 473 (2009) 20–24.
[37] P. Blaha, K. Schwarz, G.K.H. Madsen, D. Kvasnicka, J. Luitz, WIEN2k, an Augmented Plane Wave Plus Local Orbitals Program for Calculating Crystal Properties, Vienna University of Technology, Austria, 2001.
[38] J.P. Perdew, S. Burke, M. Ernzerhof, Phys. Rev. Lett. 77 (1996) 3865.
[39] O.K. Andersen, Phys. Rev. B12 (1975) 3060.
[40] J.P. Perdew, Y. Wang, Phys. Rev. B 45 (1992) 13244.
[41] J.P. Perdew, K. Burke, M. Ernzerhof, Phys. Rev. Lett. 77 (1996) 3865.
[42] C. Guzmán-Afonso, S.F. León-Luis, J.A. Sans, C. González-Silgo, P. Rodríguez-Hernández, S. Radescu, A. Muñoz, J. López-Solano, D. Errandonea, F.J. Manjón, U.R. Rodríguez-Mendoza, V. Lavín, J. Phys. Condens. Matter 27 (2015) 465401.
[43] K. Schwarz, P. Blaha, Comput. Mater. Sci. 28 (2003) 259.
[44] P.E. Blöchl, O. Jepsen, O.K. Andersen, Phys. Rev. B Condens Matter 49 (23) (1994) 16223–16233.
[45] F. Wooten, Optical Properties of Solids, Academic Press, New York and London, 1972.
[46] D.R. Penn, Phys. Rev. B 128 (1962) 2093.
[47] G.D. Boyd, H. Kasper, J.H. McFee, IEEE J. Quantum Electron 7 (1971) 563.
[48] Ph.D. thesis, Ali Hussain Reshak, Indian Institute of Technology-Rookee, India (2005).